Time-Resolved, In Situ X-ray Diffraction Studies of Staging during Phosphonic Acid Intercalation into $[LiAl_2(OH)_6]Cl{\cdot}H_2O$

Gareth R. Williams, Alexander J. Norquist,† and Dermot O'Hare*

Inorganic Chemistry Laboratory, South Parks Road, Oxford OX1 3QR, U.K.

Received October 21, 2003. Revised Manuscript Received January 2, 2004

Intercalation of a range of phosphonic acids into $[LiAl_2(OH)_6]Cl{\cdot}H_2O$ at pH 8 leads to co-intercalation of both mono- and dianionic guest anions. Solid-state ^{31}P NMR data can be used to show that these materials exhibit a ^{31}P chemical shift that is intermediate between the values for the monoanionic and dianionic forms of the respective acids, suggesting that rapid proton exchange occurs between the intercalated anions. It is possible to calculate the relative amounts of mono- and dianionic species present using the observed averaged chemical shift of the intercalate phase. In the case of methylphosphonic acid, the ratio of mono- and dianionic species ($MePO_3H^-/MePO_3^{2-}$) is estimated to be 2.1. The intercalation of methyl-, ethyl-, phenyl-, and benzylphosphonic acids into $[LiAl_2(OH)_6]Cl{\cdot}H_2O$ was studied using time-resolved, in situ energy-dispersive synchrotron X-ray diffraction. The rates of intercalation are significantly greater for methylphosphonic acid (MPA), ethylphosphonic acid (EPA), and benzylphosphonic acid (BPA) than for phenylphosphonic acid (PPA). The large BPA anions intercalate the most quickly, and MPA reacts more rapidly than EPA. Kinetic analyses of the rate data suggest that these are diffusion-controlled reactions. In situ X-ray diffraction experiments performed with slow addition of the guest have allowed observation of intermediate crystalline phases during the reactions with MPA and BPA. The intermediate phases can be indexed assuming a second-stage intercalation compound in which alternate interlayer regions are occupied by phosphonic acid and Cl^- anions, respectively (Williams et al. *Chem. Commun.* **2003**, 1816). The observation of these second-stage intermediates is very surprising, because staging in rigid layer lattices such as layered double hydroxides (LDHs) is highly unusual.

Introduction

Intercalation has long been of interest to scientists, because it allows the electronic, magnetic, and optical properties of solid host matrixes to be modified with minimal change to the structure.[1−3] Layered double hydroxides (LDHs) are attractive hosts for intercalation reactions, as they consist of positively charged layers and charge-balancing anions in the interlayer regions. These anions can be exchanged for other guest species. LDHs typically have the formula $[M_2^{2+}M^{3+}(OH)_6]^+X_{1/n}{}^{n-}{\cdot}mH_2O$. $[LiAl_2(OH)_6]Cl{\cdot}H_2O$ (LiAl LDH) is unique among LDHs in that it is the only stable LDH to contain +1 and +3 metal centers: all other LDHs contain di- and trivalent metal cations. Also, the cation ordering present in the LiAl LDH is unusual in LDH chemistry.[4] Generally, the two types of metal cations in the layers are completely disordered. In contrast, LiAl LDH is synthesized from the reaction of LiCl with gibbsite [γ-$Al(OH)_3$], and the Li^+ cations occupy the remaining octahedral sites in the γ-$Al(OH)_3$ layers in an ordered fashion. LDHs have a number of desirable properties: for example, $[LiAl_2(OH)_6]Cl{\cdot}H_2O$ has been shown to exhibit shape-selective ion exchange,[5−7] and certain LDHs are known to have catalytic properties.[3,8] Some contemporary applications of LDHs have recently been reviewed by O'Hare et al.[9]

The mechanisms by which intercalation occurs in layered hosts are still far from clear. It is generally believed that the reaction is initiated at crystal defects on the surface on the solid host; therefore, differences in reactivity are commonly observed between batches of host. To gain more insight into the reaction processes, O'Hare and co-workers have developed an environmental chemical reaction cell that allows for the study of intercalation reactions using in situ diffraction methods.[10,11] This has two major advantages over conven-

* To whom correspondence should be addressed. E-mail: dermot.ohare@chem.ox.ac.uk.

† Present Address: Department of Chemistry, Haverford College, Haverford PA, 19041.

(1) Yamanaka, S.; Kawaji, H.; Hotehama, K.; Ohashi, M. *Adv. Mater.* **1996**, *8*, 771.
(2) Reichle, W. *J. Catal.* **1985**, *94*, 547.
(3) Cavini, F.; Trifiro, E.; Vaccari, A. *Catal. Today* **1991**, *11*, 173.
(4) Besserguenev, A. V.; Fogg, A. M.; Francis, R. J.; Price, S. J.; O'Hare, D.; Isupov, V. P.; Tolochko, B. P. *Chem. Mater.* **1997**, *9*, 241.
(5) Lei, L.; Vijayan, R. P.; O'Hare, D. *J. Mater. Chem.* **2001**, *11*, 3276.
(6) Lei, L. X.; Millange, F.; Walton, R. I.; O'Hare, D. *J. Mater. Chem.* **2000**, *10*, 1881.
(7) Millange, F.; Walton, R. I.; Lei, L. X.; O'Hare, D. *Chem. Mater.* **2000**, *12*, 1990.
(8) Chibwe, M.; Valim, J. B.; Jones, W. *NATO ASI Ser., Ser. C.* **1993**, 191.
(9) Khan, A. I.; O'Hare, D. *J. Mater. Chem.* **2002**, *12*, 3191.
(10) Evans, J. S. O.; Francis, R. J.; O'Hare, D.; Price, S. J.; Clarke, S. M.; Flaherty, J.; Gordon, J.; Nield, A.; Tang, C. C. *Rev. Sci. Instrum.* **1995**, *66*, 2442.
(11) Clark, S. M.; Nield, A.; Rathbone, T.; Flaherty, J.; Tang, C. C.; Evans, J. S. O.; Francis, R. J.; O'Hare, D. *Nucl. Ins. Methods* **1995**, *97*, 98.

10.1021/cm0350434 CCC: $27.50
Published on Web 02/14/2004

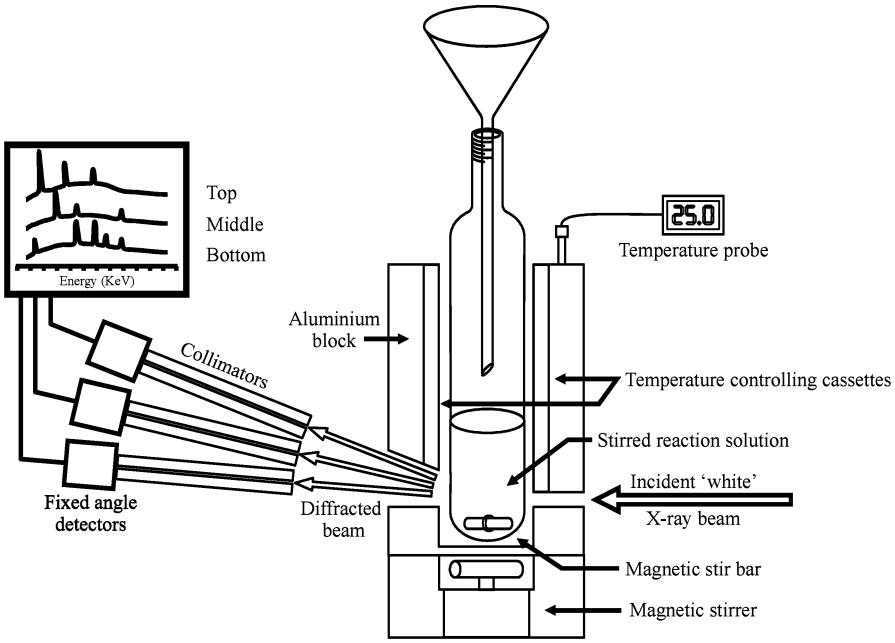

Figure 1. Experimental apparatus used to perform time-resolved in situ EDXRD experiments.

tional quenching experiments. First, whereas it has been shown that quenched products do not necessarily reflect the reaction matrix at the time of quenching, this in situ probe is noninvasive. Second, in situ experiments allow reactions to be continuously monitored, and a much greater amount of data can be collected. We have already exploited time-resolved in situ diffraction methods to study a variety of intercalation reactions.[12−19]

Time-resolved, in situ energy-dispersive X-ray diffraction (EDXRD) is particularly suitable for the study of these reactions because the simultaneous observation of a wide range of *d* spacings is possible. An energy-discriminating detector is positioned at a fixed angle to a white synchrotron X-ray beam, and the full spectral width of the beam is used to record diffraction peaks; hence, the Bragg reflections are separated by their energies.[20] The detector monitors the number of photons diffracted by the reaction mixture as a function of energy. This is in contrast to angle-dispersive diffraction where the radiation source has a fixed wavelength and a moving detector is used to record diffraction peaks, meaning that the Bragg reflections are separated by a spatial coordinate.

Each crystalline phase involved in an intercalation reaction will give rise to its own distinct set of Bragg reflections. In principle, it is possible to simultaneously observe host, product, and any crystalline intermediates that might form during these reactions. The diffraction data can be used to quantitatively determine the kinetics of these processes and gain new insight into the mechanism of these heterogeneous reactions.

Here, we describe a complete study of the intercalation of a range of phosphonic acids into $[LiAl_2(OH)_6]Cl{\cdot}H_2O$ and an investigation into the kinetics and mechanisms of these reactions using EDXRD; a preliminary report of this work was published previously.[21]

Experimental Details

Reagents. Phosphonic acids were purchased from Lancaster and were used as supplied. $[LiAl_2(OH)_6]Cl{\cdot}H_2O$ was synthesized by reacting γ-$Al(OH)_3$ with a 4-fold excess of LiCl at 90 °C for 48 h.[22]

Synthesis. Potassium salts of phosphonic acids were synthesized by preparing a solution of the acid at an appropriate pH (midway between pK_1 and pK_2 for the monoanion and above pK_2 for the dianion) using KOH solutions and then evaporating the water. Typically, 5 mL of a 0.28 M solution of the phosphonic acid at the appropriate pH (pH 8 unless otherwise stated) was added to a suspension of 0.15 g of $[LiAl_2(OH)_6]Cl{\cdot}H_2O$ in 3 mL of water. The mixture was stirred for 5 h, and then the product was isolated by filtration, washed with water and acetone, and dried under vacuum for 1−2 h.

Time-Resolved in Situ Energy-Dispersive X-ray Diffraction (EDXRD) Experiments. Experiments were carried out on Station 16.4 of the U.K. Synchrotron Radiation Source (SRS) at the Daresbury Laboratory.[10] The SRS operates with an average stored current of 200 mA and a typical beam energy of 2 GeV. A wiggler magnet working at a peak field of 6 T supplies Station 16.4 with X-ray frequency radiation. The usable X-ray flux is continuous in the range 5−120 keV, with a maximum flux of 3×10^{10} photons s^{-1} at approximately 13 keV. A three-element detector system is employed. Each detector is separated by approximately 2° in 2θ and covers a different range of *d* spacings. Some overlap exists between detectors, thereby ensuring that no Bragg reflections are missed.

Intercalation reactions were performed in glass ampules contained within a temperature-controlled block (Figure 1).[23]

(12) Fogg, A. M.; Dunn, J. S.; O'Hare, D. *Chem. Mater.* **1998**, *10*, 356.
(13) Fogg, A. M.; Dunn, J. S.; Shyu, S. G.; Cary, D. R.; O'Hare, D. *Chem. Mater.* **1998**, *10*, 351.
(14) Fogg, A. M.; Green, V. M.; Harvey, H. G.; O'Hare, D. *Adv. Mater.* **1999**, *11*, 1466.
(15) Fogg, A. M.; O'Hare, D. *Chem. Mater.* **1999**, *11*, 1771.
(16) O'Hare, D.; Evans, J. S. O.; Fogg, A.; O'Brien, S. *Polyhedron* **2000**, *19*, 297.
(17) O'Hare, D.; Fogg, A.; Green, V. M.; Harvey, H. G. *Mol. Cryst. Liq. Cryst.* **2000**, *341*, 1099.
(18) O'Hare, D.; Fogg, A.; Harvey, H. *Abstr. Pap. Am. Chem. Soc.* **1999**, *218*, 238-INOR.
(19) O'Hare, D.; Fogg, A.; Harvey, H. *Abstr. Pap. Am. Chem. Soc.* **1999**, *217*, 233-IEC.
(20) Gibbs, G. V. *Am. Mineral.* **1982**, *67*, 421.
(21) Williams, G. R.; Norquist, A. J.; O'Hare, D. *Chem. Commun.* **2003**, 1816.
(22) Fogg, A. M.; Rohl, A. L.; Parkinson, G. M.; O'Hare, D. *Chem. Mater.* **1999**, *11*, 1194.

Table 1. Kinetic Rate Equations Used to Model Diffusion-Controlled Reactions

growth model	equation
1D diffusion	$\alpha^2 = kt$
2D diffusion	$(1 - \alpha)\ln(1 - \alpha) + \alpha = kt$
3D diffusion	$[1 - (1 - \alpha)^{1/3}]^2 = kt$

Temperatures between approximately 3 and 90 °C can be accessed using this apparatus. (An alternative cell is employed for reactions at higher temperatures.) EDXRD spectra were collected at a fixed detector angle of ca. 2° in 2θ with an acquisition time of 30 s. The products were filtered, dried, and characterized using powder X-ray diffraction (XRD), elemental analysis (EA), IR spectroscopy, thermogravimetric analysis (TGA), and solid-state NMR spectroscopy.

Data Analysis. An automated Gaussian fitting routine is used to obtain the peak areas of the Bragg reflections.[24] These values are subsequently converted to the extent of reaction at time t, $\alpha(t)$, defined as $\alpha(t) = I_{hkl}(t)/I_{hkl}(\max)$, where $I_{hkl}(t)$ is the area of a given peak at time t and $I_{hkl}(\max)$ is the maximum area of this peak.

A number of expressions have been developed to allow for the modeling of the growth curves observed experimentally for solid-state reactions. The most commonly used is the Avrami−Erofe'ev expression.[25−27] This expression divides the reaction into separate stages of product nucleation and nuclei growth; it has the general functional form

$$\alpha(t) = 1 - \exp[-(kt)^m] \qquad (1)$$

This expression is found to be most applicable in the range $0.15 < \alpha < 0.8$. The exponent m can (in favorable instances) be used to deduce information about the rate of nucleation and the mechanism of nuclei growth;[28] k is the rate of reaction. The value of m can most easily be obtained using a Sharp−Hancock plot,[29] which is a plot of $\ln[-\ln(1 - \alpha)]$ vs ln(time) and gives a straight line of gradient m and intercept $m \ln k$. Alternative expressions exist to model diffusion-controlled reactions. Different kinetic models are used for 3D, 2D, and 1D diffusion, as summarized in Table 1.[30]

Powder X-ray Diffraction. Powder XRD patterns were recorded on a Philips PW1729 diffractometer in reflection mode at 40 kV and 30 mA, using Cu Kα radiation.

Infrared Spectroscopy. Infrared spectroscopy experiments were carried out using a Perkin-Elmer 1600 series FTIR spectrometer. Samples were mixed with KBr and made into pellets, and spectra were recorded between 4000 and 400 cm^{-1}. Thirty-two scans were recorded with a scan resolution of 4 cm^{-1}.

Thermogravimetric Analysis. TGA measurements were performed on a Rheometric Scientific STA-1500H instrument. Approximately 20 mg of sample was heated in a platinum crucible between 25 and 800 °C at a heating rate of 10 °C/min under a stream of argon.

Solid-State NMR Spectroscopy. Solid-state magic angle spinning (MAS) ^{31}P NMR spectra were recorded on a Varian Chemagnetics CMX Infinity 200 MHz spectrometer. Spectra were recorded at ambient temperature, with the sample mounted in a 7.5-mm double-resonance MAS probe.

Results and Discussion

Synthesis and Characterization of LDH/Phosphonic Acid Intercalation Compounds.

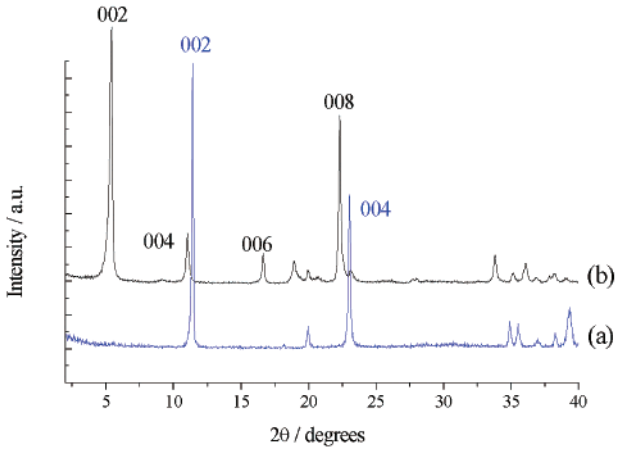

Figure 2. Powder XRD patterns of (a) $[LiAl_2(OH)_6]Cl{\cdot}H_2O$ and (b) the reaction product of $[LiAl_2(OH)_6]Cl{\cdot}H_2O$ and phenylphosphonic acid.

Table 2. Phosphonic Acid Intercalates of Li/Al LDH Synthesized at pH 8

phosphorus oxyacid	intercalation compound	d_{002} (Å)
none (host material)	$[LiAl_2(OH)_6]Cl{\cdot}H_2O$	7.70
methylphosphonic acid	$[Li_{0.84}Al_2(OH)_6](MePO_3)_{0.19}(MePO_3H)_{0.46}{\cdot}2.6H_2O$	12.7
ethylphosphonic acid	$[Li_{0.88}Al_2(OH)_6](EtPO_3)_{0.28}(EtPO_3H)_{0.33}{\cdot}2.4H_2O$	13.8
phenylphosphonic acid	$[Li_{0.85}Al_2(OH)_6](PhPO_3)_{0.1}(PhPO_3H)_{0.65}{\cdot}2.7H_2O$	15.7
benzylphosphonic acid	$[Li_{0.89}Al_2(OH)_6](BzPO_3)_{0.15}(BzPO_3H)_{0.58}{\cdot}2.2H_2O$	16.9

Addition of an excess of the phosphonic acids derived from either methylphosphonic acid (MPA), ethylphosphonic acid (EPA), phenylphosphonic (PPA), or benzylphosphonic acid (BPA) to a suspension of $[LiAl_2(OH)_6]Cl{\cdot}H_2O$ in water at room temperature (RT) and pH 8 leads to rapid ion exchange of the Cl^- ions and intercalation of the phosphonate anions. In the isolated solid products, an absence of the characteristic Bragg reflections of the $[LiAl_2(OH)_6]Cl{\cdot}H_2O$ host in the powder XRD patterns and a lack of Cl in the elemental microanalyses (EAs) of the solids were observed. The powder XRD pattern of the product of the reaction of $[LiAl_2(OH)_6]Cl{\cdot}H_2O$ with $PhPO_3H_2$ (PPA) is shown in Figure 2. This powder XRD could be indexed using a hexagonal unit cell with $a =$ 5.1 Å and $c = 31.4$ Å, giving an interlayer separation of 15.7 Å. A full listing of the EA data and interlayer spacing for all of the phosphonic acid intercalates synthesized at pH 8 is presented in Table 2.

The Li/Al ratio in the products is less than 0.5 (as determined using elemental analysis), as a result of some Li^+ being leached from the LDH structure into solution. This phenomenon has been observed on numerous other occasions when we have intercalated organic anions into $[LiAl_2(OH)_6]Cl{\cdot}H_2O$. The loss of lithium from the metal layers is believed to compensate for the lower charge density in the anion layer caused when the larger organic anions replace the chloride ions. The analytical data indicate that the intercalation compounds contain a mixture of both mono- and dianionic guest anions. Although there is literature precedent for the intercalation of either the mono or dianionic phosphonic acid guest in layered hosts,[31,32] the co-intercalation of both species has not been studied

(23) Neild, A. A.; Hammond, W. B.; Abram, D.; Bates, A.; Wilkinson, P. J.; Taylor, D. J., manuscript in preparation.
(24) Clark, S. M. *J. Appl. Cryst.* **1995**, *28*, 646.
(25) Avrami, M. *J. Chem. Phys.* **1940**, *8*, 212.
(26) Avrami, M. *J. Chem. Phys.* **1941**, *9*, 177.
(27) Erofe'ev, B. V.; Dokl, C. R. *Acad. Sci. URSS* **1946**, *52*, 511.
(28) Hulbert, S. F. *J. Br. Ceram. Soc.* **1969**, *6*, 11.
(29) Hancock, J. D.; Sharp, J. H. *J. Am. Ceram. Soc.* **1972**, *55*, 74.
(30) Francis, R. J.; O'Brien, S.; Fogg, A. M.; Halasyamani, P. S.; O'Hare, D.; Loiseau, T.; Ferey, G. *J. Am. Chem. Soc.* **1999**, *121*, 1002.

thoroughly. pH titrations were carried out on MPA, and it was determined that this diacid had p$K_1 \approx 5$ and p$K_2 \approx 10$. Therefore, at pH 8, both the monoanionic and dianionic forms of the acid will be present in the solution, enabling the intercalation of both species. To confirm the coexistence of the monoanionic and dianionic forms of the guest ions, solid-state ^{31}P MAS NMR spectroscopy was used to determine the chemical shift of the phosphorus atom in the intercalates of methylphosphonic acid (MPA) and phenylphosphonic acid (PPA), as well as the shifts in the mono- and dipotassium salts of MPA and the neutral compound.

Both the MPA and PPA intercalates exhibit a single ^{31}P resonance that is intermediate between the values for the monoanionic and dianionic forms of the respective acids. The single ^{31}P signal present in each spectrum suggests that rapid proton exchange is occurring between the mono- and dianionic species. It is possible to calculate the relative amounts of mono- and dianionic species present from the chemical shift of the intercalate phase. For MPA intercalation, the $MePO_3H^-/MePO_3^{2-}$ ratio was calculated to be 2.1; this compares well to the ratio of 2.4 from elemental analysis. For PPA, the NMR ratio was found to be $PhPO_3H^-/PhPO_3^{2-} = 5.7$, as compared to a ratio of 6.5 determined by EA.

Thermogravimetric analysis was performed on the phosphonic acid intercalates to determine the amount of water co-intercalated. Three mass losses were observed in the TGA trace for the intercalates; for the PPA intercalate, the first mass loss between approximately 45 and 180 °C (ca. 15.3%) is attributed to the loss of 2.7 equiv of interlayer water, giving $[Li_{0.85}Al_2(OH)_6](PhPO_3)_{0.1}(PhPO_3H)_{0.65}$. The second mass loss of ca.16.1% between 180 and 380 °C corresponds to the dehydration of the lattice, producing $[Li_{0.85}Al_2O_3](PhPO_3)_{0.1}(PhPO_3H)_{0.65}$. The final mass loss of 16.5% between 560 and 700 °C corresponds to the loss of the organic part of the phosphonic acid, giving a phase with the approximate formula $Li_{0.85}Al_2O_{5.35}P_{0.75}$. Very similar results are seen for the intercalates of methyl-, ethyl-, and benzylphosphonic acids.

A number of bands characteristic of phosphonate units are present in the IR spectra of the intercalates.[32] In the spectrum of the PPA intercalate, there is a sharp P−C stretching vibration at 1438 cm^{-1} and vibrations of the O_3P-C group at around 1000 cm^{-1}. Peaks characteristic of the monosubstituted phenyl ring at 753, 723, and 694 cm^{-1} are also visible in the spectrum, as are O−H vibrations at ca. 3500 cm^{-1} and peaks at approximately 950, 740, and 550 cm^{-1} owing to vibrations of the $[LiAl_2(OH)_6]^+$ layers.[33] Similar bands are seen in the IR spectra of the MPA, EPA, and BPA intercalates.

Performing the intercalation reactions at different pHs causes the ratio of monoanionic/dianionic phosphonic acid anions to vary. In the case of the MPA system, a distinctly different product is observed when the reaction is performed at pH = 10 (11.1 Å basal spacing, as opposed to the 12.7 Å spacing seen at lower pH). The phase of lower *d* spacing seen at pH 10 can be rationalized because the intercalate contains entirely dianionic MPA. Thus, the number of anions needed to balance the layer charge is smaller than at lower pH. The lower density of anions in the interlayer region results in the lower *d* spacing. It also explains why less Li^+ leaches from the LDH structure at higher pH; at lower pH values, it is not physically possible to fit enough anions into the interlayer region to balance the charge of the layers, and therefore, Li^+ leaches from the structure to ensure electroneutrality. The lower density of interlayer anions at higher pH is expected to be responsible for the greater amount of co-intercalated water, as more space is available in the interlayer region with lower anion density.

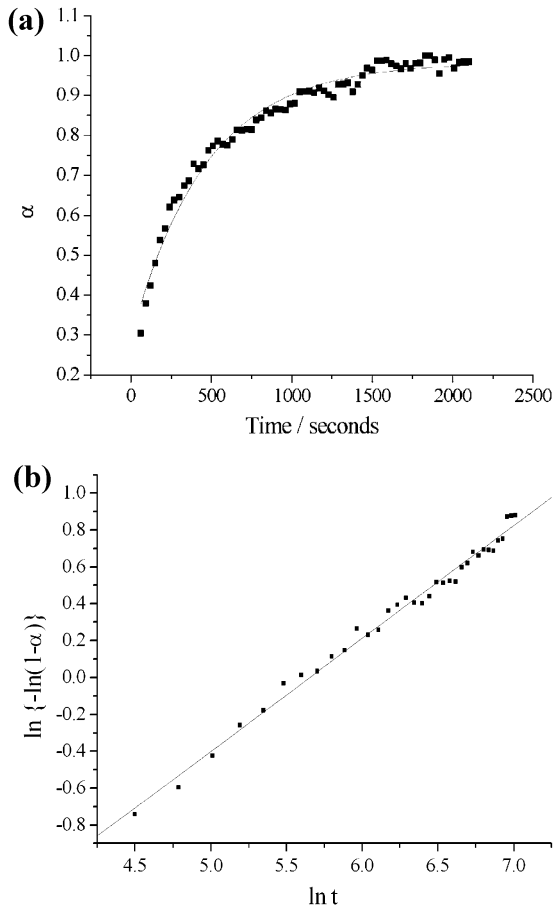

Figure 3. (a) Evolution of the d_{002} peak of the PPA intercalate with time at 26.5 °C. (b) Sharp−Hancock plot for the intercalation of PPA at 26.5 °C.

Time-Resolved in Situ Powder Diffractions Studies. *Intercalation of PPA in $[LiAl_2(OH)_6]Cl\cdot H_2O$.* The intercalation of the anions derived from PPA was studied over a range of temperatures using time-resolved in situ EDXRD. The (004) Bragg reflection of the intercalate and the (002) Bragg reflection of the host occur at approximately the same *d* spacing (ca. 8 Å) and were not fully resolved in the EDXRD experiment. This means that the decay of the host peak cannot be reliably used for kinetic analysis. A typical curve showing the increase in peak intensity of the (002) reflection of the PPA intercalate with time is shown in Figure 3a. The kinetic parameters determined from Sharp−Hancock analysis are summarized in Table 3.

(31) Prevot, V.; Forano, C.; Besse, J. P. *Appl. Clay Sci.* **2001**, *18*, 3.
(32) Nijs, H.; Clearfield, A.; Vansant, E. F. *Microporous Mesoporous Mater.* **1998**, *23*, 97.
(33) Isupov, V. P. *J. Struct. Chem.* **1999**, *40*, 672.

Table 3. Kinetic Data for the Intercalation of PPA into $[LiAl_2(OH)_6]Cl{\cdot}H_2O$

temp (°C)	m^a	k^a (10^{-3} s^{-1})
3.8	0.97	0.33
8.1	0.75	1.2
9.6	0.61	1.4
16	0.5	2.9
26.5	0.62	3.5

[a] m is the order of reaction, and k is the rate of reaction found from least-squares fitting of the Sharp−Hancock equation $\{\ln[-\ln(1-\alpha)] = m\ln(t) + m\ln(k)\}$.

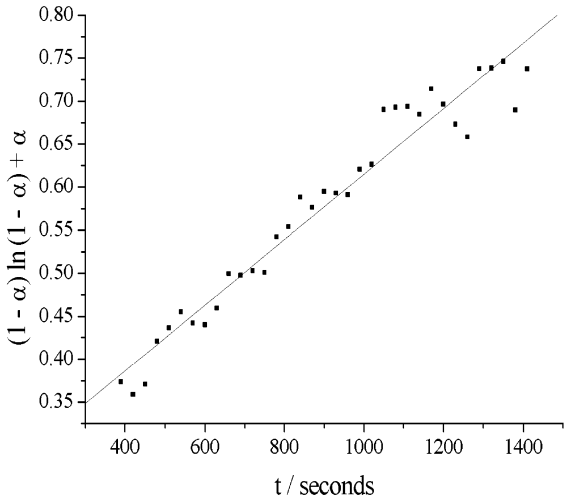

Figure 4. Plot of $(1-\alpha)\ln(1-\alpha) + \alpha$ vs t for the intercalation of PPA at 26.5 °C.

The Sharp−Hancock plots are linear, indicating that the reaction proceeds via a consistent mechanism over the course of the reaction. At higher temperatures, the exponent m is found to be approximately 0.5, indicating a diffusion-controlled process. As soon as the phosphonic acid anions reach the host lattice, they intercalate, replacing the chloride anions. However, as the temperature is lowered, m increases to approximately 1, suggesting that, at lower temperatures, the reaction is nucleation controlled. The rate-determining step of the reaction is now the expansion of the interlayer space to accommodate the phosphonic acid anions, rather than the diffusion of the phosphonic acid anions to the host. This change can be attributed to the lower energy of the system as the temperature is lowered. At 8.1 °C, m is 0.75, implying that, at this temperature, the two possibilities are equally favorable. The equations in Table 1 were used to investigate whether a diffusion growth model is applicable at higher temperatures. The plot of $[(1-\alpha)\ln(1-\alpha) + \alpha]$ vs t (Figure 4) is linear at 9.6, 16, and 26.5 °C, meaning that the reaction is 2D diffusion controlled at these temperatures. This corresponds to diffusion into the interlamellar regions. The other possible diffusion-controlled models in Table 1 produced markedly nonlinear plots.

Intercalation of Other Phosphonic Acids in $[LiAl_2(OH)_6]Cl{\cdot}H_2O$. The rapid rates of intercalation of methylphosphonic acid (MPA), ethylphosphonic acid (EPA), and benzylphosphonic acid (BPA) meant that less kinetic information was obtained. In addition, rapid decay of the host Bragg reflections meant that reliable integrated reflection intensity data could be obtained only for the growth of the product phase. These data are provided in the Supporting Information.

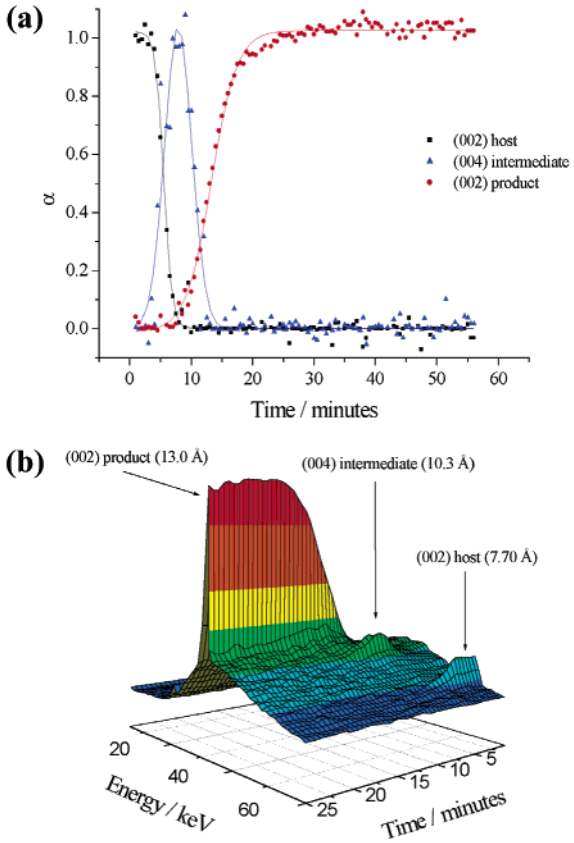

Figure 5. Time-resolved in situ EDXRD data showing the course of the ion-exchange reaction between $[LiAl_2(OH)_6]Cl{\cdot}H_2O$ and MPA at pH 8.

The exponent m is approximately 0.5 for all of these reactions, suggesting a diffusion-controlled process. At comparable temperatures, the rate of reaction is much greater for the intercalation of MPA, EPA, and BPA than for PPA. Perhaps surprisingly, the large BPA anions intercalate the most quickly, and MPA intercalates more rapidly than EPA. This trend is explained by considering the fact that the activation energy for the reaction will be affected by both the expansion in the basal spacing of the host and the extent of solvation of the potential guest molecules. Thus, the rate of reaction will be determined by a balance of these factors. These reactions are also 2D diffusion controlled.

In Situ EDXRD Studies of Slow Addition of Phosphonic Acid to $[LiAl_2(OH)_6]Cl{\cdot}H_2O$. In a separate series of experiments, the intercalation of the four phosphonic acids was studied with slow addition of the acid to the LDH suspension. The rate of reaction is then limited by the speed of guest addition, and so, no kinetic parameters can be obtained. However, the slow addition of the guest ions can sometimes allow for the detection of transient intermediate phases. A syringe pump was used to add the guest solution dropwise to the host. A pump speed of 0.225 mL min^{-1} was used to add 9 mL of a 0.28 M phosphonic acid solution to the host over ca. 40 min.

Slow Addition of Methylphosphonic Acid to $[LiAl_2(OH)_6]Cl{\cdot}H_2O$. In situ EDXRD experiments were performed on the intercalation of MPA at four different pH values, owing to the presence of pH-dependent phases. The results of the pH 8 experiment are shown in Figure 5.

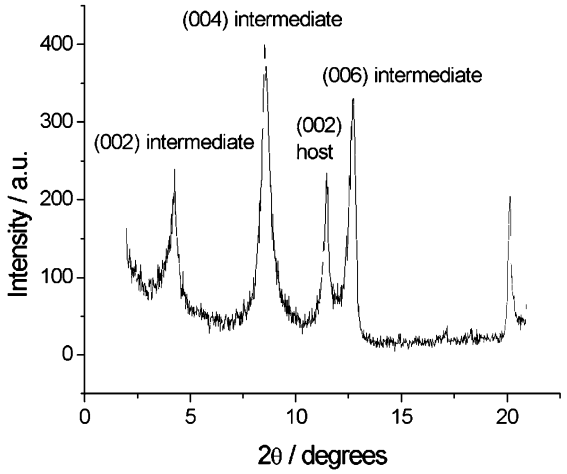

Figure 6. Powder XRD pattern showing the presence of a second-stage intercalate.

In all four cases, the reaction proceeds from the host to the product via a crystalline intermediate. As the reaction pH is increased, the amount of phosphonic acid solution required to complete the reaction and form the first-stage intercalate (i.e., the intercalate with all interlayer regions occupied by phosphonic acid anions) decreases. This is a result of the higher average charge on each MPA anion at higher pH.

It is clear that the reaction proceeds via the same intermediate at all pH values. The products have the same d spacing at each pH (13.0 Å). This is slightly higher than the value observed ex situ for pH < 10, because the intercalates are more hydrated when studied in situ. The same product d spacing is seen for pH 10. Because analysis of the powder XRD pattern of the pH 10 reaction product after drying gave $d_{002} = 11.1$ Å, it can be inferred that the 13.0 Å phase observed in situ is due to a more hydrated form of the intercalate. Upon drying, some water is extruded from the interlamellar region, and the anions rearrange to produce the lower d spacing phase.

The formation of an intermediate is both interesting and rare in LDH chemistry.[12,21,34] To gain more insight into the nature of the intermediate, the reaction was repeated and quenched at the point where the concentration of intermediate was expected to be greatest. This did not allow for the isolation of the intermediate as a single phase, but the powder XRD pattern of the quenched material contains a Bragg reflection at 20.7 Å, as well as reflections at 10.4 and 7.7 Å. The latter peak is due to incomplete reaction of the host, and the former peaks can be assigned as the (002) and (004) reflections, respectively, of a second-stage intercalate (this has alternate interlayer regions occupied by MPA and Cl). This phase would have $d_{002} = d_{002}(\text{LDH}-\text{Cl}) + d_{002}(\text{LDH-MPA}) = 7.7 + 13.0 = 20.7$ Å and, hence, $d_{004} = 10.4$ Å. The powder XRD pattern of the quenched material is shown in Figure 6. It is likely that the low intensity of the (002) peak of the intermediate prevented it from being observed in situ. The formula $[Li_{0.8}Al_2(OH)_6](MePO_3H)_{0.4}Cl_{0.4}\{[Li_{0.8}Al_2(OH)_6]Cl\}_{0.3}\cdot 3.5H_2O$ was calculated for the quenched material from elemental analysis data. The second-stage intercalate is shown in Figure 7.

Slow Addition of Benzylphosphonic Acid to $[LiAl_2(OH)_6]Cl\cdot H_2O$. The intercalation of benzylphosphonic acid (BPA) into $[LiAl_2(OH)_6]Cl\cdot H_2O$ as monitored using EDXRD is shown in Figure 8. The intercalation of BPA proceeds via an intermediate that has a d spacing of 12.2 Å. Quenching experiments allow for the isolation of a phase containing both host and intermediate reflections, as seen in the powder XRD pattern of this material. Reflections are observed at 7.7 Å [host (002)] and at 12.2 and 24.4 Å. These latter peaks are assigned to the (004) and (002) reflections, respectively, of a second-stage intercalate.

Slow Addition of Ethylphosphonic Acid to $[LiAl_2(OH)_6]Cl\cdot H_2O$. The intercalation of ethylphosphonic acid (EPA) into $[LiAl_2(OH)_6]Cl\cdot H_2O$ proceeds directly to the product without going through any intermediate phases.

Slow Addition of Phenylphosphonic Acid to $[LiAl_2(OH)_6]Cl\cdot H_2O$. Intercalation is seen to proceed directly from the host to the product.

Conclusions

Organic phosphonate anions readily intercalate into the LDH $[LiAl_2(OH)_6]Cl\cdot H_2O$. The precise nature of the intercalated anions is dependent on the pH of the reaction. Time-resolved in situ EDXRD experiments provide a useful insight into the mechanism and kinetics of the intercalation reactions. All of these intercalation reactions are observed to proceed as soon as guest solution is added to the host suspension: there is no induction period. Phenylphosphonic acid intercalates much more slowly than methyl-, ethyl-, and benzylphosphonic acids.

A diffusion-controlled mechanism is observed in the intercalation of MPA, EPA, and BPA. A shift from a 2D

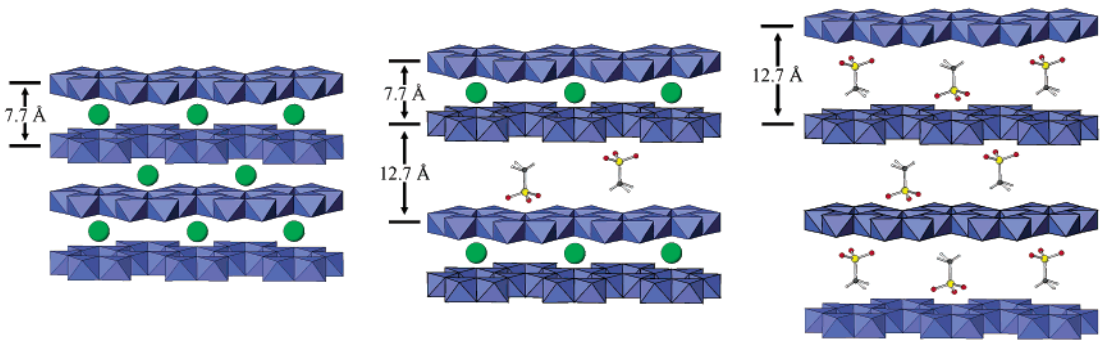

Figure 7. Schematic showing the intercalation of methylphosphonic acid into Li/Al LDH: (a) $[LiAl_2(OH)_6]Cl\cdot H_2O$, (b) second-stage intermediate featuring alternate layers occupied by Cl and MPA anions, and (c) first-stage product with all interlayer regions occupied by MPA.

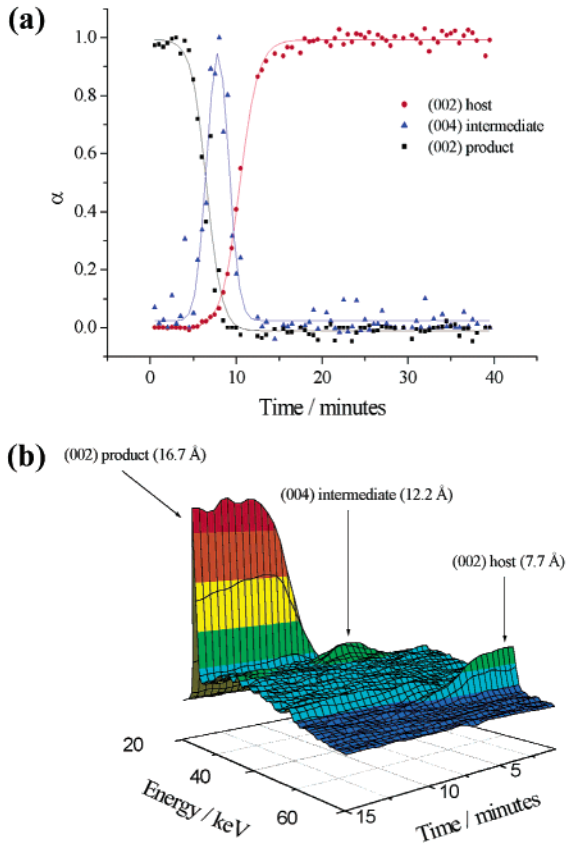

Figure 8. EDXRD data showing the intercalation of BPA into $[LiAl_2(OH)_6]Cl{\cdot}H_2O$: (a) plot showing the evolution of the host, intermediate, and product (002) Bragg reflections with time; (b) 3D stacked plot showing the host (002) Bragg reflection and the intermediate and product (002) and (004) Bragg reflections.

diffusion-controlled to a nucleation-controlled mechanism is observed at 8 °C in the reaction with PPA. The intercalation of MPA and BPA clearly occurs in a two-stage process, whereby the first-stage product is formed via a second-stage intermediate. A detailed study of the intercalation of MPA over a wide pH range (pH 4−10) shows the reaction to proceed via the same intermediate in all cases. It seems, therefore, that the cointercalation of mono- and dianionic guest anions and the relative amounts of each anion present do not affect the reaction mechanism or the intermediates formed.

It is unclear at present why an intermediate is seen with MPA and BPA but not with EPA and PPA. Subtle differences in structure and the way in which the guests are arranged in the interlayer spaces will affect the energies of the first- and second-stage species, and a balance of these factors must exist to determine whether it is kinetically more advantageous to proceed from the host to the product directly or via a second-stage intermediate. To understand exactly the intercalation process, detailed calculation of the lattice energies of the various species involved in the reaction is necessary. Unfortunately, this is not possible with systems of this complexity.

Acknowledgment. The authors thank Dr Nick Rees for help with the solid-state NMR experiments and the EPSRC and Worcester College, Oxford, U.K., for financial support.

Supporting Information Available: The following Supporting Information is available: (1) solid-state ^{31}P MAS NMR data for MPA and PPA species; (2) thermogravimetric analysis plot of $[Li_{0.85}Al_2(OH)_6](PhPO_3)_{0.1}(PhPO_3H)_{0.65}{\cdot}2.7H_2O$; (3) IR spectrum of $[Li_{0.85}Al_2(OH)_6](PhPO_3)_{0.1}(PhPO_3H)_{0.65}{\cdot}2.7H_2O$; (4) table summarizing the MPA-containing intercalates synthesized at different pH's; (5) kinetic data for the intercalation of MPA, EPA, and BPA into $[LiAl_2(OH)_6]Cl{\cdot}H_2O$; and (6) time-resolved EDXRD data for the slow addition of MPA to $[LiAl_2(OH)_6]Cl{\cdot}H_2O$ at different pH. This material is available free of charge via the Internet at http://pubs.acs.org.

CM0350434

(34) Iyi, N.; Kurashima, K.; Fujita, T. *Chem. Mater.* **2002**, *14*, 583−589.